Egyptian Knowledge Bank
https://ijmti.journals.ekb.eg/

International Journal of Materials Technology and Innovation
Volume 2, Issue 2 (2022), pages 1-12

Online ISSN 2682-4299

2D Transition Metal Dichalcogenides for Energy Applications

Fayza A. Ali, Ahmed Mourtada Elseman*, Mahmoud Rasly, Ali Omar Turky and Mohamed M. Rashad

Electronic & Magnetic Materials Department, Advanced Materials Institute, Central Metallurgical Research and Development Institute (CMRDI), Helwan, P.O. Box 87, Cairo 11421, Egypt.

*Corresponding author: E-mail: AhmedMourtada5555@yahoo.com (A. M. Elseman)

Received 21 August 2022
Accepted 12 October 2022
Published 31 December 2022

Abstract

The potential of transition metal dichalcogenides (TMDCs) in nano energy has garnered considerable interest. Layered materials from the transition metal dichalcogenides provide 2D systems a rich, mainly unexplored source of diversity. Exfoliation or vapour phase deposition techniques may be used to create better the right-sized, adjustable-thickness, and better transition metal dichalcogenides layers electrical and optical characteristics. Due to their very high surface areas and electrical characteristics, semiconducting transition metal dichalcogenides monolayers have been shown to be practical for various energy-related applications, including nanogenerators, energy storage, electrocatalytic hydrogen synthesis, and green electronics. In this review, we first describe the structure including surface growth as morphology, domain size and grain boundaries and orientation, characteristics, and preparation including top-down and bottom-up methods. Top-down method as liquid exfoliation and mechanical cleavage, bottom-up method as chemical exfoliation, chemical vapor deposition, and solvothermal before going into great depth about the creation of Applications for nano energy based on transition metal dichalcogenides.

Keywords: Transition Metal Dichalcogenides, Surface Growth of Materials, Top-Down synthesis, Bottom-Up synthesis, Energy applications

1. Introduction

Due to the scarcity of fossil fuels, green energy foundations are generally acknowledged as the only practical solution to guarantee the long-term growth of the global economy and society. Due to their erratic nature, renewable energy sources provide power (such as solar, wind, and hydraulic), making it difficult to utilize them effectively and consistently. New energy-generating and storage technologies have received much attention. The 3D-perovskite halides have set themselves apart from similar semiconductor materials because they achieved a remarkable high-power conversion efficiency of 25.2% within a decade [1]. As organometal halide perovskite has intense photoluminescence (PL) emission, which plays a good role in energy applications, affecting solar cell efficiency [2-4] 3-arylazo-thieno[3,2-b] good possibilities for p-type electronics include pyranone dyes (hole transport layer) [5]. A simple one-step hydrothermal process successfully created carbon and nitrogen co-doped MoS_2 nanoflakes [6]. Perovskites have effectively used chalcogenide quaternary electronics as an inorganic hole-transport component [7, 8]. Electronics with "low power consumption and great performance" are needed for intelligent and effective energy use. Due to their intriguing basic features and possible energy applications, transition metal dichalcogenides (TMDCs) in two dimensions (2D) have received a lot of interest [9-15]. A transition metal M layer is sandwiched between two atomic layers of chalcogens X in a one-layer TMDC, which belongs to the family of layered materials known as 2D TMDCs. TMDC layers only exhibit weak van der Waals interactions with one another, similar to graphene.

The weak interlayer coupling also alters their electrical structures, which is interesting since TMDCs exhibit major changes in their properties as they approach one monolayer thick. Numerous prospective

green energy applications, including as energy production [16], energy storage [17-20], catalysis [21-25], and electronic devices [10], may be facilitated by monolayer 2D TMDCs. They are able to achieve this because of unique basic characteristics that have never been seen in their bulk counterparts. Only a few of the special features of monolayer semiconducting TMDCs with a direct band gap include strong interactions with light [26, 27], valley-dependent physics [28], strong piezoelectric coupling [16, 29, 30], and a high current on-off ratio for field effect transistors [31]. These special qualities of 2D TMDCs open up a wide range of possibilities for their use in the nano energy sector. TMDCs are attractive active materials in piezoelectric nano energy generators because to their high piezoelectric coupling, which is similar to that of conventional bulk wurtzite structures. Optoelectronics based on TMDCs are anticipated to have the benefits of rapid responses, compactness, low weight, and energy efficiency. The existing electronics industry may undergo a full transformation because of the TMDC-based transistor's significant promise for low power consumption products [10].

In order to investigate the possibility of material band-structure engineering for cutting-edge energy applications like solar energy harvesting [32, 33], electrochemical energy storage [17], and catalytic energy conversion[21, 22], these materials' properties can also be changed through doping, surface adsorption, straining, and interaction with other materials. Therefore, notably in the field of nano energy, 2D TMDCs has emerged as one of the most active study fields. Transition metal compounds have many applications as photodegradation for example it was obtain that methyl green with Fe(II)-o-phenthroline incorporated into zeolite reach up 45.4% of photocatalytic degradation, AgBr and g-C_3N_4 semiconductor material enhancement the activity of photocatalytic and the CdS-AgBr nanocomposite in the degradation of methylene blue showed good activity in photocatalytic also transition metal compounds have effective applications as heavy qualifications by using electrochemical sensors, drug delivery [34-43]. We discuss the production, characteristics, and prospective applications of 2D TMDCs in a variety of nano-energy systems in this paper.

2. Material synthesis

Nowadays, many methods are used to synthesized two dimensions transition metal dichalcogenides (2d TMDCS) [44, 45]. There are mainly two approaches, top-down synthesis [46] and bottom-up synthesis. The top-down synthesis includes three methods mechanical cleavage, liquid exfoliation [47, 48], and chemical exfoliation [49-51]. The bottom-up synthesis involves other two methods as chemical vapor deposition (CVP) [52, 53] and solvo-thermal synthesis [54, 55].

2.1 Top-Down synthesis

2.1.1 Mechanical Cleavage

Mechanical cleavage is the top-down synthesis that occurs most often. In this technique, the bulk crystal is transformed into a monolayer or few-layer structure using the adhesive force of scotch tape [44, 56, 57]. Advantages and drawbacks of mechanically exfoliated ultrathin 2D TMDCs are present. The ultrathin 2D TMDCs are manufactured by mechanical cleavage to produce huge, crystalline nanosheets with minimal flaws that are used in electrical devices and basic research on the physicochemical characteristics of matter. The pace of manufacturing is minimal, and it is challenging to regulate the size and thickness. The nanosheet needs the substrate to be supported. The 2D TMDCs that this approach generates are challenging to use in biomedicine [58]. The exfoliation behavior of layered compounds has been studied for more than 50 years, such as the mechanical exfoliation of smectite clay minerals in aqueous solution to obtain single layers of clay and the physical exfoliation of graphite into single layer graphene as shown in Fig. 1. The host materials, or the layered materials, which consist of 2D platelets weakly stacked to form 3D structures, such as graphite and MoO_3 [59, 60].

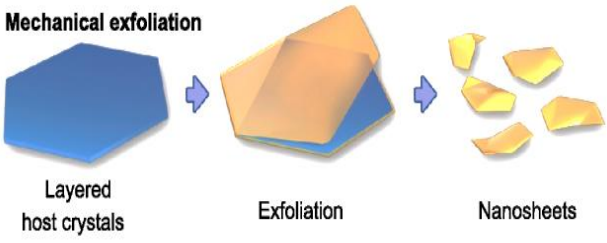

Fig. 1 Demonstrates how stacked host materials are mechanically exfoliated. Reproduced with permission from Ref. [61].

2.1.2 Liquid Exfoliation

A further common top-down synthesis is liquid exfoliation. This technique may demonstrate that bulk crystals were successfully exfoliated using ultrasonic energy in a particular solvent [62-65]. Since the contact generated by sonicating is the week van der Waals, yet

weak covalent connections in-plane cannot be broken, the appropriate ultrasonic intensity and duration are crucial for accomplishing the optimal exfoliation of bulk crystals. Solvent molecules primary roles are to produce exfoliated nanosheets and prevent reassembling.

Solvent molecules with the proper surface energy adhere to nanosheet surfaces via the van der Waals interaction. To improve exfoliation efficiency, the degree of compatibility between solvent molecules and nanosheets is crucial. The most popular organic solvents are N-methyl-pyrrolidone (NMP) and dimethylformamide (DMF) [66]. The several ultrathin 2D TMDCs that have been created so far via liquid exfoliation are MoS_2 [64], WS_2 [48], $NbSe_2$, $TeSe_2$, and $NiTe_2$ [47]. By addressing certain mechanical cleavage shortcomings, liquid exfoliation enables the mass production of ultrathin 2D TMDCs with favourable photoelectric characteristics. But since it's difficult to make single-layer 2D TMDCs using this technique, organic solvents are undesirable in the applications that come after. The experimental setup for the bulk synthesis of monolayer 2D TMDCs liquid exfoliation could realize successful exfoliation of bulk crystals via ultrasonication in specific solvent shown in Fig. 2.

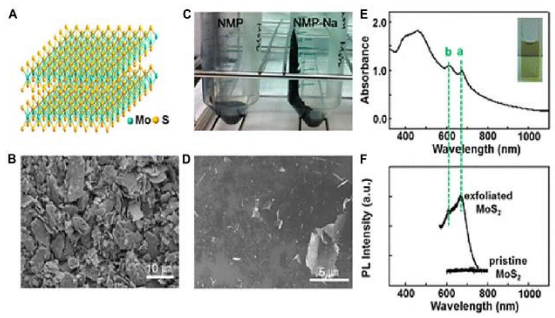

Fig. 2 Liquid-based exfoliation of bulk MoS_2. The MoS_2 crystal structure is depicted in (A), along with (B) SEM images of pure MoS_2 powder, (C) a photo image demonstrating the impact of exfoliation with NaOH (on the right side) and without NaOH (on the left, the control sample), (D) a SEM image of exfoliated MoS_2 nanosheets with NaOH in NMP, (E) a UV-vis spectrum (with an inset photo image of the MoS_2 dispersion (F)The characteristics of a 2H-MoS_2 nanosheet may be responsible for the "a" and "b" peaks, which are representative of the smallest direct transition. Reproduced with permission from Ref [64].

2.1.3 Chemical Exfoliation

Chemical exfoliation employs ultrasonication in water and intercalators to effectively exfoliate the bulk crystals' interlayer [49, 67]. This method involves first intercalating the intercalators into the interlayer of bulk TMDCs in ethanol or water, and then sonicating the bulk TMDCs to exfoliate them into ultrathin nanosheets. The most common intercalators consist of organometallic substances like butyllithium, naphthyl sodium, etc. The quantity of intercalators and their insertion into the bulk TMDCs generated by the battery were set up by adjusting the voltage [50]. In biomedicine, chemical exfoliation is utilised to make ultrathin 2D TMDCs without the use of safe solvents. The direct synthesis of free-standing SnO/SnO_2 and ZnO ultrathin nanosheets via mechanical exfoliation or combined chemical intercalation and liquid exfoliation has shown in Fig. 3 Machado et al. have synthesized bimodal ZnO nanostructures with ZnO nanosheet decorated by dodecylsulphate intercalation of zinc hydroxy salt, $Zn_5(OH)_8(DS)_2 \cdot mH_2O$ [68, 69].

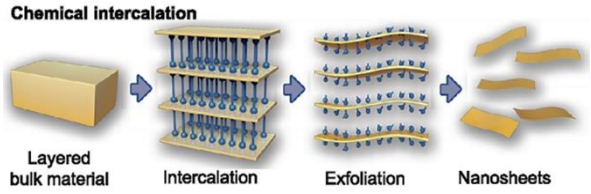

Fig. 3 Shows chemical intercalation-induced exfoliation. Reproduced with permission from Ref. [61].

2.2 Bottom-Up synthesis

2.2.1 Chemical Vapor Deposition (CVD)

A classic bottom-up synthesis is CVD. High temperature and high pressure are used throughout exposing the reaction process via reaction precursors to the substrate. The precursors provide the chalcogenide and transition metal atoms, which generate ultrathin 2D TMDCs by reaction. The ultrathin 2D TMDCs are created when the reaction product is subsequently applied to the substrate [51, 53, 70, 71]. This technique produces an ultrathin 2D TMDCs nanosheet with excellent electrical properties and superior crystal quality. However, this process requires a high vacuum and temperature. The substrate is also used to improve the transfer of nanosheets. Normally, a two-step thermolysis process was used to obtain high-quality thin film, as shown in Fig. 4(a) [51]. After dip-coating of $(NH_4)_2MoS_4$ on substrates, Ar/H_2 mix flow were introduced and kept at relative low temperature and low pressures (500 °C, 1 Torr) for an hour to remove the residual solvent, NH_3, H_2S and other byproducts; then at second step of annealing, high

temperature (1000 °C) and additional sulfur were applied to improve the crystallinity and electrical performance. The extra sulfur helped to remove excess oxygen and mitigate sulfur deficit caused by organic solvent evaporation. As shown in Fig. 4(b), in a typical growth, rhomboidal MoO_2 microplates nucleated and grew on substrate through thermally evaporation, and then reduced by sulfur vapor at 650– 850 °C, then MoO_2 were sulfurized to MoS_2 layer-by-layer at higher temperature to control number of layers [53]. As shown in Fig. 4(c), high quality MoS_2 was deposited on insulating substrate (placed at cooler zone, ~650 °C) via vapor–solid growth mechanism under Ar gas [72].

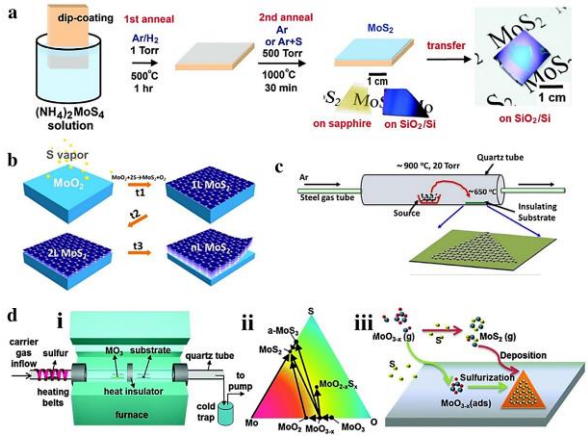

Fig. 4 Demonstrates 4 possible development paths for TMDCs. (a) two-step thermolysis technique is used to create $(NH_4)_2MoS_4$ from a precursor on SiO_2/Si or sapphire substrates. This process is then transferred onto another substrate after going through two phases of annealing on insulating substrates. (b) the layer-by-layer transfer of MoS_2 from MoO_3 to a different substrate by surface sulfurization. (c) using a straightforward vapour transport method and an ambient atmosphere, MoS_2 films were created on an insulating substrate at a high temperature. (d) (i) low pressure CVD system setup for TMDCs (ii) Mo-O-S Ternary phase diagram illustrating the CVD development of MoS_2 from precursors of MoO_3 (iii) and possible growth pathways of MoS_2 through the reaction of MoO_{3-x} and S. Reproduced from Reference with permission [51, 53, 72, 73].

In Fig. 4(d(i)), synthesizing TMDs materials by CVD method involves vapor phase reaction of two precursors e.g., transition metal oxides/halides and chalcogen precursors. This kind of CVD process is classified into atmospheric pressure CVD (APCVD), modified metal–organic CVD (MOCVD) and low-pressure CVD (LPCVD). For CVD growth of MoS_2 from MoO_3 and sulfur powder, the Mo–O–S ternary phase diagram as shown in Fig. 4(d(ii)). It has been considered that MoO_3 reacts with sulfur and produces MoS_2 as shown in Fig. 4(d(iii)) [73], and according to the following equations

$$2MoO_3 + xS \rightarrow MoO_{3-x} + xSO_2$$

$$2MoO_{3-x} + (7 - x)S \rightarrow xMoS_2 + (3 - x)SO_2.$$

Nevertheless, several researchers have found that H_2 also plays a vital role for the growth of TMDs. It acts as an additional reducing agent with Se during the growth of $MoSe_2$ nanosheets [74]. High quality single crystalline 3R-$MoTe_2$ were synthesized by CVD method and using $MoCl_5$ as Mo precursor [75].

2.2.2 Solvo-Thermal Synthesis

Another bottom-up synthesis is solvo-thermal synthesis. By using appropriate solvent and reaction time conditions, this approach produces ultrathin 2D TMDCs from precursors [54, 76, 77]. Thiourea interacts with molybdic or tungstic acid for three hours at 773 K. The end product contains very thin MoS_2 or WS_2 nanosheets. This method's strength has ability to create ultrathin 2D TMDCs with high yield and at a cheaper cost. Bismuth (Bi) possesses high X-ray attenuation in computed tomography (CT) imaging [78], as it shows a dose-enhanced capability in tumor RT [79, 80]. Bi-containing composites have been widely researched in biomedical applications. Bi atoms show a strong photoelectric absorbance capacity under X-ray radiation and can generate numerous short-range secondary electrons, thus enhancing the X-ray deposition in tumor tissues and accelerating the DNA breaking. Ammonium tetra-thiomolybdate ($(NH_4)_2MoS_4$) has been introduced in the solvo-hydrothermal production of MoS_2 nanosheets and NPs [81]. production of 2D polyethylene glycol (PEG)-ylated MoS_2 nanosheets by solvothermal treatment of $(NH_4)_2MoS_4$ and PEG-400 aqueous solution for tumor PTT [82]. Wang et al., inspired by the stoichiometric proportion of Mo and S atoms in $(NH_4)_2MoS_4$ to design a reaction with two extra S atoms and Bi atoms during the solvothermal treatment, to obtain MoS_2 /Bi_2S_3-PEG (MBP) composite nanosheets MoS_2/Bi_2S_3-PEG (MBP) nanosheets As shown in Fig. 5 [83]. exhibited broad absorption in the NIR region. As MoS_2/Bi_2S_3-PEG (MBP) nanosheets dispersions to the NIR laser at a pre-determined power density to explore the correlation of the photothermal performance with the concentration, irradiation time and power density.

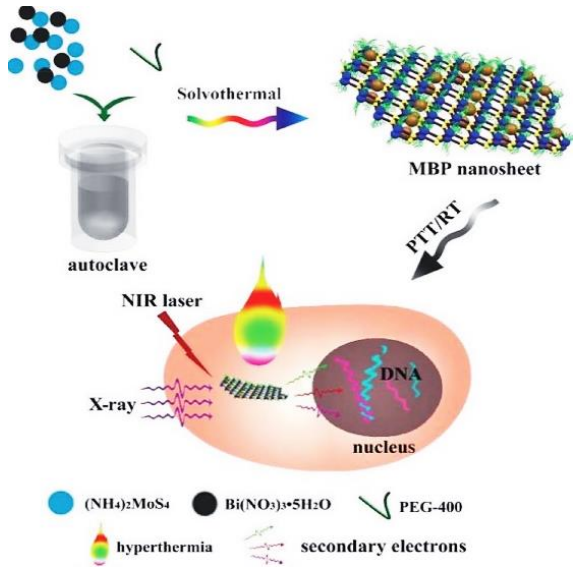

Fig. 5 The solvothermal production of MoS_2/Bi_2S_3-PEG (MBP) nanosheets, tumour photothermal treatment (PTT), and radiation are shown schematically (RT). Reproduced with permission from Ref.[83]

3. Surface Growth of Materials

The scalable synthesis of TMDCs layers with consistently excellent quality has been authorised due to the potential uses in electrical and optoelectronic devices. High crystallinity, large domain, few grain boundaries and defect-freeness are all examples of high quality. Large-scale uniform MoS_2 layers' quality is greatly influenced by structural elements such grain boundaries, morphology, and orientation.

3.1 Morphology

Morphological control is essential for ensuring good quality and high performance for applications in electrical and optoelectronic features when synthesising high-quality TMDCs on a large scale. The CVD process has been used to create single-layered TMDCs with a variety of morphologies, including triangles, stars, pentagons, and hexagons [84]. Numerous studies have shown that the substrates, gas flow velocity, temperature, precursors ratio and concentration all have an impact on the form of the TMDCs layers as they develop. For instance, it was discovered that hydrogen has a significant impact on the morphologies of TMDCs during development and that a little quantity of H_2 gas may be used to modify the morphology from jagged-like structures to straight edge and monolayer triangle [85]. The same is true when the H_2 concentration rises. Likely due to the deposition of W atoms onto Se edges, more WO_3 is reduced by H_2 as H_2 concentration rises, resulting in the formation of volatile WO_{3-X}. While the right fluxes of WO_{3-x} and Se result in the creation of hexagons with great selectivity or triangles with W/Se edges by managing the H_2 pressure [75]. Additionally, the regulation of MoS_2 morphology is significantly impacted by the distance between the metal source and substrate, which controls the concentration of vapour metal precursor [86]. MoS_2 changes from a medium-sized truncated triangle of 6 metres to a huge triangle of 50 metres when the distance between it and the precursor increases, before rising to a medium-sized truncated triangle of 2 to 3 metres as in Fig. 6(a). As the development rate of various edge terminations substantially influences the characteristics of this form. The ratio of Mo to S changed to 1:2 when the growth rates of the various edge terminations became equal, producing the hexagonal form. Otherwise, when the ratio of Mo to S exceeds 1:2, the tendency of S atoms to form bonds with free Mo atoms causes S zigzag termination to develop more quickly than Mo zigzag termination, resulting in the final structure of twisted triangles. However, when the ratio of Mo to S is less than 1:2 and the concentration of Mo vapour falls, the S vapour gradient becomes tiny and the substrate moves far from the Mo source, resulting in S zigzag triangles. When crystal orientation is determined by optical microscopy, Mo zigzag triangle is more effective because its edges are crisp and straight than the S zigzag triangle [87]. According to the Kinetic Monte Carlo simulation, MoS_2 will change in size and form depending on the precursor concentration Fig.6(b) [88].

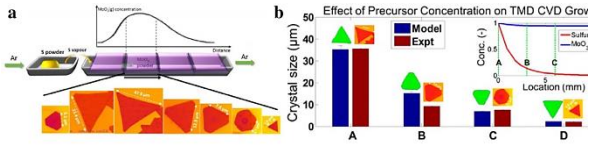

Fig. 6 Displays the control over shape of TMDCs materials. (a) MoS_2 CVD growing system, to start. The MoS_2 may be seen in a variety of sizes and forms in the optical pictures. (b) Theoretical and experimental measurements of the effects of precursor concentration on the sizes and forms of TMDCs during CVD development. Reproduced with permission from Ref. [86, 88]

3.2 Domain size and grain boundaries

Using CVD synthesis, the grain size of large-scale polycrystalline MoS_2 film can be adjusted up to micrometres. The Raman spectra exhibited almost little variation in peak location and intensity as the grain size rose from 20 to 600 nm, but band-gap adjustment

allowed for the detection of PL shift. Additionally, as the grain size was decreased, there was greater scattering at the grain borders, which lowered the carrier mobility. The thermal conductivity of CVD-grown polycrystalline MoS_2 has recently decreased at the low-angle grain boundaries. The grain size and the nucleation density are strongly connected [89]. The following equation illustrates the relationship between the source and growth distance (d) with thermodynamic and kinetic growth factor the concentration of gaseous MoS_2 (C_g):

$$C_g(d,t) = C_g(0,t)\exp\left(-\frac{d^2}{4Dt}\right)$$

equation1 where t is time and D is the diffusion constant.

The average domain size and surface coverage as a function of distance are shown in Fig. **7**(a) [90].

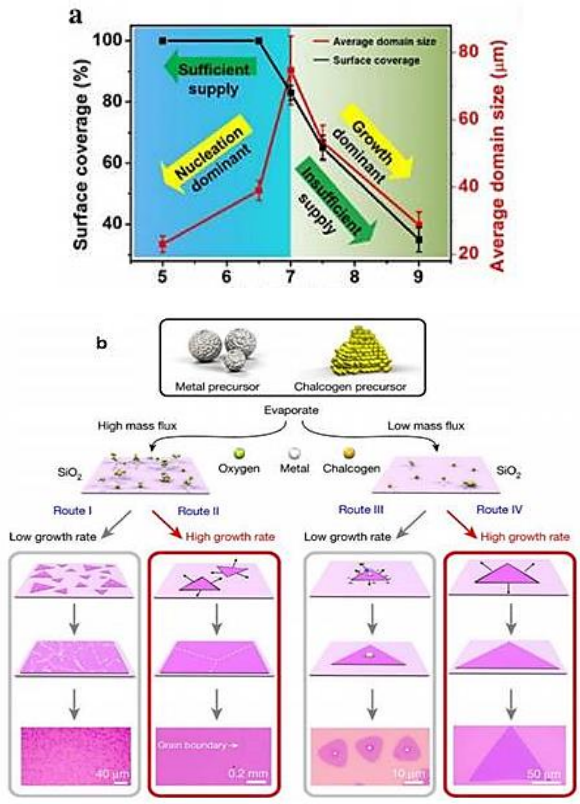

Fig. 7 Controlled by grain size and limits. As a precursor/substrate distance, MoS_2's surface coverage and average domain size. (a) Surface coverage and average domain size of MoS_2 as a function of precursor/substrate distance. (b) Flow diagram shows different ways for the synthesis of distinct types TMDCs by the chemical vapor deposition method. Different routes indicated the nucleus formation and their growth mechanism as a function of mass flux of precursor and growth rate Ref [90, 91].

Numerous tiny MoS_2 domains adapt and overlap at the border with high surface coverage as a result of the distance of less than 7 mm demonstrating high C_g adequate source supply and high nuclei distance. The biggest single crystal size (>300μm) was demonstrated under the conditions of an adequate source supply and a high nuclei density (d = 7 mm). However, when (d > 7 mm), C_g decreases as a result of the limited source supply, average domain size and surface coverage both decline [59]. Fig. **7**(b) divided into four routes depending on the growth of 2D TMDCs that change by changing the mass flux and the growth rate [91]. In route (I), while the mass flux is high, the growth rate is low to obtain a polycrystalline film with many grain boundaries and small grain size. Route (II) as the mass flux is high, and the growth rate is high, which causes smooth monolayer film with limited grain boundaries and large grain size. Route (III) as the mass flux is low, the growth rate is low, and so it is suitable for a single crystalline with a small domain. Route (IV), while the mass flux is low, the high growth rate showed a large monolayer single crystalline [91]. The grain boundary affects the quality of layered TMDCs so it's an important factor [92].

3.3 Orientation

Different misorientations of neighbouring grains create grain borders, which therefore allow for the formation of various electronic structures [93]. As is well known, the quality of TMDCs reduced as electrical devices by deforming the grain boundaries due to the high misorientation angle. In a similar vein, grain orientation control is crucial as a grain-size controlled technique. It allows for the production of well aligned 2D TMDC growth and creates homogeneous layers of a large area. Two processes have been explained by the prevalent 60° misorientations. There were a few pre-aligned 2D islands at 60° in the first mechanism, while random island orientation was dragged into 60°in the second mechanism by capillary forces [94]. Today, a large number of aligned growths have been successfully completed on single crystal substrates such as c-plane (0010) facet sapphire, mica, or GaN [95]. These substrates provided guidance for TMDCs growth orientation by step edges at relatively high temperature or through van der Waals interaction as the substrate and TMDCs lattice matched [96].

The low potential energy between the tiny MoS_2 seeds and the c-plane sapphire substrate has also been mentioned as a possible explanation for how the little MoS_2 seeds were able to spin to advantageous

orientations so quickly (0°, 60°). However, during the first nucleation process, the ratio of precursors (S, MoO_3) determines the shape of a rotatable seed (Fig. 8(a)) [97].

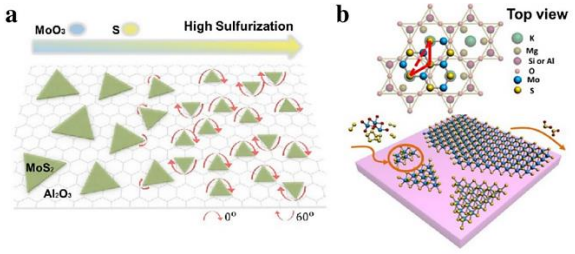

Fig. 8 The orientation control of TMDs materials is done during the first nucleation processes. (a) MoS_2 seed rotation in relation to the precursor ratio (S/MoO_3). (b) MoS_2 epitaxial growth on the surface of mica. Reproduced with permission from Ref. [97, 98].

The triangular MoS_2 seeds were predominantly aligned along two opposed orientations [98, 99], and mica substrate was employed in the synthesis as illustrated in Fig. 8(b). The virtually lattice-matching property seems to have led to a much-reduced growth temperature (530 °C). Furthermore, studies revealed that a high hydrogen concentration promoted the development of an active Al-rich sapphire surface, which improved the interaction between sapphire and WS_2 and led to the production of a well-oriented triangle and a successful stitch of merged grains [100].

4. Energy Applications

2D TMDCs are employed in solar cells by forming a Schottky or p-n junction, which acts as the interface for segregating charge carriers. Too important at this time of the Schottky junction kind, the TMDC semiconductor is in contact with a metal or graphene contact. The power conversion efficiency (PCE) of the An Interfacial solar cell made of a metal (Au) base and MoS_2 nanomembrane was measured at 1.8 percent for stacks of MoS_2 that were around 220 nm thick [101]. With a multilayer graphene contact and a WS_2 nanosheet with a thickness of around 37 nm, A greater PCE of 3.3 percent might be generated using WS_2/graphene-based solar cells [102]. Contrary to projections that TMDC absorbs 5–10% of incoming sunlight to be around one order more than GaAs and Si of the very same thickness (1 nm), an ultrathin solar cell composed of MoS_2/graphene layered monolayers may attain a PCE of around 1% in just 1 nm thickness [33].

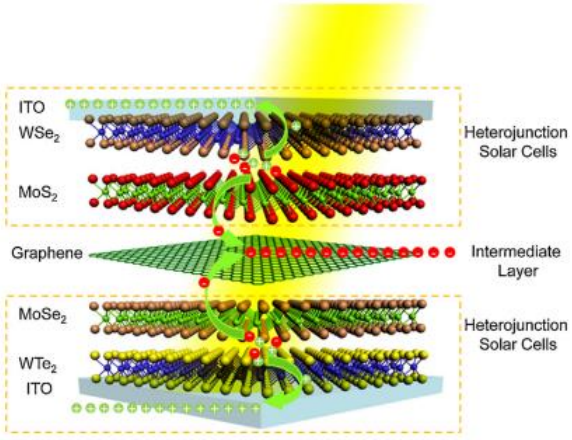

Fig. 9 Diagram of a solar cell using parallel-connected tandem TMDCs. The TMDCs heterojunction photovoltaics $MoSe_2/WTe_2$ (1.18–1.58 eV) and MoS_2/WSe_2 (1.61–1.89 eV) have similar.complementary absorption windows that are joined together using graphene as an intermediary layer. Graphene and ITO anodes effectively separate and extract photo-excited electrons and holes. Reproduced with permission from Ref. [103].

A monolayer WSe_2 p-n diode's PCE is estimated to be about 0.5 percent [104]. A layer photovoltaic cell with layered MoS_2 and WSe_2 layers have a PCE of 0.2% [105]. The n-type monolayer MoS2's quantum efficiency (EQE) is high, p-type silicon heterostructure exceeds 4% [106], and the MoS_2/Si-based photovoltaic systems could achieve a high PCE of over 5% [32]. By stacking TMDCs with With graphene serving as the intermediate, distinct band gaps linking them as photovoltaic devices with energies varying from optical to near-infrared, as shown in Fig. 9, it is possible to overcome the inherent limitations enforced by the thin layers' narrow optical absorption paths [103, 107]. TMDCs can be used as hole extraction buffer layers or catalytic counter electrode (CE) materials in the photovoltaic industry and as photoactive semiconductor layers [108]. A comparatively high PCE of 8.11 percent may be achieved [109] by integrating ultrathin, an effective hole-extraction layer for photovoltaic devices made on 2D MoS_2 nanosheets.

The transition metal dichalcogenides (TMDCs) have applications in Photoelectrochemical (PEC) water splitting which can produce water electrolysis which can lower overpotential and speed up absorption of light energy [110, 111]. The combunation of MoS_2 with graphene enhance condutivity as the graphene make conducting network between the MoS_2 and substrate electrode [21]. The transition metal dichalcogenides (TMDCs) can use for energy storage as it not need high charge carrier mobility like other

electronics-based applications as CVD method can control morphology and gives heterojunctions in lateral or vertical geometries with seamless atomic stitching of sub-atomic layers [112, 113]. The transition metal dichalcogenides (TMDCs) has application in energy generation as Photovoltaics as it has direct bandgap energies and broad optical absorptions in a range of infrared to visible light, Semiconducting 2D TMD layers [33]. p-type organic semiconductors such as C8-BTBT were described to epitaxially grow on the top of n-type 2D MoS_2 monolayers, achieving PV p-n junctions [114].

5. Conclusion

The energy problem is one of the most pressing and vital in our contemporary civilization. In order to lessen our over-dependence on non-renewable fossil fuels, there has been an increase in the need for energy storage and conversion technologies that are economical, effective, and ecologically beneficial. In this case, TMDCs have shown tremendous promise. Recent developments in components for monolayer 2D TMDCs, including characterization and the creation of devices, have benefited the research of related 2D materials. Layered materials have long been understood and researched. The development of nano energy applications, including photovoltaics, H_2 production, piezoelectric, and lithium-ion batteries, may be facilitated by the unique features of 2D TMDCs. Other 2D TMDCs are receiving increasing attention, and it is hoped that innovative new applications will soon emerge.

References

[1] A. E. Abd El-Samad et al., Mixed 2D-3D Halide Perovskite Solar Cells. Sol. Cells Theory Mater. Recent Adv, (2021) 163-184.

[2] M. M. Rashad, A.M. Elseman, and A.M. Hassan, Facile synthesis, characterization and structural evolution of nanorods single-crystalline $(C_4H_9NH_3)$ $2PbI_2X_2$ mixed halide organometal perovskite for solar cell application. Optik, 127(20), (2016) 9775-9787.

[3] A. M. Elseman et al., Copper-substituted lead perovskite materials constructed with different halides for working (CH_3NH_3) $2CuX_4$-based perovskite solar cells from experimental and theoretical view. ACS applied materials & interfaces, 10(14), (2018) 11699-11707.

[4] A. M. Elseman, L. Luo, and Q.L. Song, Self-doping synthesis of trivalent Ni_2O_3 as a hole transport layer for high fill factor and efficient inverted perovskite solar cells. Dalton Transactions, 49(40), (2020) 14243-14250.

[5] A. M. Elseman et al., Molecular Modelling, Optical and Electrochemical Properties of Novel 3-Arylazo-thieno [3, 2-b] pyranone for Photovoltaic Application. Russian Journal of General Chemistry 92(6), (2022) 1121-1128.

[6] M. G. Fayed et al., Carbon and nitrogen co-doped MoS_2 nanoflakes as an electrode material for lithium-ion batteries and supercapacitors. Sustainable Materials and Technologies, 29, (2021) e00306.

[7] M. Sanad et al., Facile synthesis of sulfide-based chalcogenide as hole-transporting materials for cost-effective efficient perovskite solar cells. Journal of Materials Science: Materials in Electronics, 30(7), (2019) 6868-6875.

[8] A. M. Elseman and M. Rashad, Influence of nitrogen atmosphere one-step heating assisted the solution processing of Kesterite $Cu2ZnSnS_4$ as hole extraction on the efficacy of the inverted perovskite solar cells. Optical Materials, 124 (2022) 111998.

[9] Y. Shi, H. Li, and L.-J. Li, Recent advances in controlled synthesis of two-dimensional transition metal dichalcogenides via vapour deposition techniques. Chemical Society Reviews, 44(9) (2015) 2744-2756.

[10] Q. H. Wang et al., Electronics and optoelectronics of two-dimensional transition metal dichalcogenides. Nature nanotechnology, 7(11) (2012) 699-712.

[11] M. Chhowalla et al., The chemistry of two-dimensional layered transition metal dichalcogenide nanosheets. Nature chemistry, 5(4) (2013) 263-275.

[12] Zhang H., ACS Nano (2015). doi. org/10.1021/acsnano. 5b05040.

[13] C. Tan, and H. Zhang, Wet-chemical synthesis and applications of non-layer structured two-dimensional nanomaterials. Nature communications, 6(1) (2015) 1-13.

[14] X. Huang et al., 25th Anniversary article: hybrid nanostructures based on two-dimensional nanomaterials. Advanced Materials, 26(14) (2014) 2185-2204.

[15] X. Huang, Z. Zeng, and H. Zhang, Metal dichalcogenide nanosheets: preparation, properties and applications. Chemical Society Reviews, 42(5) (2013) 1934-1946.

[16] W. Wu et al., Piezoelectricity of single-atomic-layer MoS_2 for energy conversion and piezotronics. Nature, 514(7523) (2014) 470-474.

[17] T. Stephenson et al., Lithium ion battery applications of molybdenum disulfide (MoS_2) nanocomposites. Energy & Environmental Science, 7 (1) (2014) 209-231.

[18] G. Sun et al., Fabrication of Ultralong Hybrid Microfibers from Nanosheets of Reduced Graphene Oxide and Transition-Metal Dichalcogenides and their Application as

Supercapacitors. Angewandte Chemie International Edition, 53(46) (2014) 12576-12580.
[19] G. Sun et al., Hybrid fibers made of molybdenum disulfide, reduced graphene oxide, and multi-walled carbon nanotubes for solid-state, flexible, asymmetric supercapacitors. Angewandte Chemie, 127(15) (2015) 4734-4739.
[20] X. Cao et al., Preparation of MoS2-coated three-dimensional graphene networks for high-performance anode material in lithium-ion batteries. small, 9(20) (2013) 3433-3438.
[21] Y. Li et al., MoS_2 nanoparticles grown on graphene: an advanced catalyst for the hydrogen evolution reaction. Journal of the American Chemical Society,133(19) (2011) 7296-7299.
[22] Y. H. Chang et al., Highly efficient electrocatalytic hydrogen production by MoS_x grown on graphene-protected 3D Ni foams. Advanced materials, 25(5) (2013) 756-760.
[23] Z. Yin et al., Au nanoparticle-modified MoS_2 nanosheet-based photoelectrochemical cells for water splitting. Small, 10(17) (2014) 3537-3543.
[24] C.-B. Ma et al., MoS_2 nanoflower-decorated reduced graphene oxide paper for high-performance hydrogen evolution reaction. Nanoscale, 6(11) (2014) 5624-5629.
[25] Y. Liu et al., Back Cover: Folding Up of Gold Nanoparticle Strings into Plasmonic Vesicles for Enhanced Photoacoustic Imaging (Angew. Chem. Int. Ed. 52/2015). Angewandte Chemie International Edition, 54(52) (2015) 15916-15916.
[26] H. Li et al., From bulk to monolayer MoS_2: evolution of Raman scattering. Advanced Functional Materials, 22(7) (2012) 1385-1390.
[27] K. F. Mak et al., Atomically thin MoS_2: a new direct-gap semiconductor. Physical review letters, 105(13) (2010) 136805.
[28] K. F.Mak et al., Control of valley polarization in monolayer MoS_2 by optical helicity. Nature nanotechnology, 7(8) (2012) 494-498.
[29] J. Qi et al., Piezoelectric effect in chemical vapour deposition-grown atomic-monolayer triangular molybdenum disulfide piezotronics. Nature communications,. 6(1) (2015)1-8.
[30] H. Zhu et al., Observation of piezoelectricity in free-standing monolayer MoS_2. Nature nanotechnology,. 10(2) (2015) 151-155.
[31] B. Radisavljevic et al., Single-layer MoS_2 transistors. Nature nanotechnology, 6(3) (2011)147-150.
[32] M.-L. Tsai et al., Monolayer MoS_2 heterojunction solar cells. ACS nano,. 8(8) (2014) 8317-8322.
[33] M. Bernardi, M. Palummo, and J.C. Grossman, Extraordinary sunlight absorption and one nanometer thick photovoltaics using two-dimensional monolayer materials. Nano letters, 13(8) (2013) 3664-3670.
[34] A. Nezamzadeh-Ejhieh, and E. Shahriari, Photocatalytic decolorization of methyl green using Fe (II)-o-phenanthroline as supported onto zeolite Y. Journal of Industrial and Engineering Chemistry,. 20(5) (2014) 2719-2726.
[35] S. Ghattavi, and A. Nezamzadeh-Ejhieh, GC-MASS detection of methyl orange degradation intermediates by AgBr/g-C_3N_4: Experimental design, bandgap study, and characterization of the catalyst. International Journal of Hydrogen Energy,. 45(46) (2020) 24636-24656.
[36] S. A.Mirsalari, A. Nezamzadeh-Ejhieh, and A.R. Massah, A designed experiment for CdS-AgBr photocatalyst toward methylene blue. Environmental Science and Pollution Research, 29(22) (2022) 33013-33032.
[37] T. Tamiji, and A. Nezamzadeh-Ejhieh, A comprehensive study on the kinetic aspects and experimental design for the voltammetric response of a Sn (IV)-clinoptilolite carbon paste electrode towards Hg (II). Journal of Electroanalytical Chemistry, 829 (2018) 95-105.
[38] T. Tamiji, and A. Nezamzadeh-Ejhieh, Electrocatalytic determination of Hg (II) by the modified carbon paste electrode with Sn (IV)-clinoptilolite nanoparticles. Electrocatalysis,. 10(5) (2019) 466-476.
[39] S. Ghattavi, and A. Nezamzadeh-Ejhieh, A visible light driven AgBr/g-C_3N_4 photocatalyst composite in methyl orange photodegradation: focus on photoluminescence, mole ratio, synthesis method of g-C_3N_4 and scavengers. Composites Part B: Engineering,183 (2020) 107712.
[40] H. Derikvandi, and A. Nezamzadeh-Ejhieh, Increased photocatalytic activity of NiO and ZnO in photodegradation of a model drug aqueous solution: effect of coupling, supporting, particles size and calcination temperature. Journal of hazardous materials, 321 (2017) 629-638.
[41] N. Omrani, and A. Nezamzadeh-Ejhieh, A novel quadripartite Cu2O-CdS-BiVO4-WO_3 visible-light driven photocatalyst: Brief characterization and study the kinetic of the photodegradation and mineralization of sulfasalazine. Journal of Photochemistry and Photobiology A: Chemistry, 400 (2020)112726.
[42] S. Ghattavi, and A. Nezamzadeh-Ejhieh, A double-Z-scheme ZnO/AgI/WO_3 photocatalyst with high visible light activity: Experimental design and mechanism pathway in the degradation of methylene blue. Journal of Molecular Liquids, 322 (2021)114563.
[43] H. Derikvandi, and A. Nezamzadeh-Ejhieh, A comprehensive study on enhancement and

optimization of photocatalytic activity of ZnS and SnS_2: Response Surface Methodology (RSM), nn heterojunction, supporting and nanoparticles study. Journal of Photochemistry and Photobiology A: Chemistry, 348 (2017) 68-78.
[44] J. Y. Huang et al., In situ observation of graphene sublimation and multi-layer edge reconstructions. Proceedings of the National Academy of Sciences,. 106(25) (2009) 10103-10108.
[45] H. Li et al., Mechanical exfoliation and characterization of single-and few-layer nanosheets of WSe_2, TaS_2, and $TaSe_2$. small,. 9(11) (2013) 1974-1981.
[46] G. Fiori et al., Electronics based on two-dimensional materials. Nature nanotechnology, 9(10)(2014) 768-779.
[47] J. W. Anderson, The production of ultrasonic sounds by laboratory rats and other mammals. Science, 119(3101) (1954) 808-809.
[48] V. Vega-Mayoral et al., Photoluminescence from liquid-exfoliated WS_2 monomers in poly (vinyl alcohol) polymer composites. Advanced Functional Materials, 26(7) (2016)1028-1039.
[49] G. Eda et al., Photoluminescence from chemically exfoliated MoS_2. Nano letters, 11(12) (2011) 5111-5116.
[50] Z. Zeng et al., Single-layer semiconducting nanosheets: high-yield preparation and device fabrication. Angewandte Chemie, 123(47) (2011) 11289-11293.
[51] K.-K. Liu et al., Growth of large-area and highly crystalline MoS2 thin layers on insulating substrates. Nano letters, 12(3) (2012) 1538-1544.
[52] F. Hui et al., Synthesis of large-area multilayer hexagonal boron nitride sheets on iron substrates and its use in resistive switching devices. 2D Materials, 5(3) (2018) 031011.
[53] X. Wang et al., Controlled synthesis of highly crystalline MoS_2 flakes by chemical vapor deposition. Journal of the American Chemical Society, 135(14) (2013) 5304-5307.
[54] Y. Peng et al., Hydrothermal synthesis of MoS2 and its pressure-related crystallization. Journal of Solid State Chemistry, 159(1) (2001) 170-173.
[55] H. Ramakrishna Matte et al., MoS_2 and WS_2 analogues of graphene. Angewandte Chemie International Edition, 49(24) (2010) 4059-4062.
[56] A. Splendiani et al., Emerging photoluminescence in monolayer MoS_2. Nano letters, 10(4) (2010) 1271-1275.
[57] I. Diez-Perez et al., Ambipolar transport in an electrochemically gated single-molecule field-effect transistor. ACS nano, 6(8) (2012) 7044-7052.
[58] Y. Chen et al., Two-dimensional graphene analogues for biomedical applications. Chemical Society Reviews, 44(9) (2015) 2681-2701.
[59] G. Walker, Macroscopic swelling of vermiculite crystals in water. Nature, 187(4734) (1960) 312-313.
[60] Z. Wang, and T.J. Pinnavaia, Hybrid organic−inorganic nanocomposites: exfoliation of magadiite nanolayers in an elastomeric epoxy polymer. Chemistry of Materials, 10(7) (1998) 1820-1826.
[61] Z. Sun, , T. Liao, and L. Kou, Strategies for designing metal oxide nanostructures. Science China Materials, 60(1) (2017) 1-24.
[62] M. B. Dines, Lithium intercalation via n-butyllithium of the layered transition metal dichalcogenides. Materials Research Bulletin, 10(4) (1975) 287-291.
[63] P. Joensen, , R. Frindt, and S.R. Morrison, Single-layer mos2. Materials research bulletin, 21(4) (1986) 457-461.
[64] G. S. Bang et al., Effective liquid-phase exfoliation and sodium ion battery application of MoS_2 nanosheets. ACS applied materials & interfaces, 6(10) (2014) 7084-7089.
[65] Y. Yong et al., WS_2 nanosheet as a new photosensitizer carrier for combined photodynamic and photothermal therapy of cancer cells. Nanoscale, 6(17) (2014)10394-10403.
[66] A. Jawaid et al., Mechanism for liquid phase exfoliation of MoS_2. Chemistry of Materials, 28(1) (2016) 337-348.
[67] M. A. Lukowski et al., Enhanced hydrogen evolution catalysis from chemically exfoliated metallic MoS_2 nanosheets. Journal of the American Chemical Society, 135(28) (2013) 10274-10277.
[68]J. Machado, N. Ravishankar, and M. Rajamathi, Delamination and solvothermal decomposition of layered zinc hydroxysalt: Formation of bimodal zinc oxide nanostructures. Solid state sciences, 12(8) (2010) 1399-1403.
[69] H. Wang et al., Polyvinylpyrrolidone-assisted ultrasonic synthesis of SnO nanosheets and their use as conformal templates for tin dioxide nanostructures. Langmuir, 28(28) (2012) 10597-10601.
[70] C.-H. Lee et al., Effects of oxidative DNA damage and genetic polymorphism of the glutathione peroxidase 1 (GPX1) and 8-oxoguanine glycosylase 1 (hOGG1) on lung cancer. Journal of Preventive Medicine and Public Health, 39(2) (2006) 130-134.
[71] X. Ling et al., Role of the seeding promoter in MoS2 growth by chemical vapor deposition. Nano letters, 14(2) (2014) 464-472.

[72] S. Wu et al., Vapor–solid growth of high optical quality MoS_2 monolayers with near-unity valley polarization. ACS nano, 7(3) (2013) 2768-2772.
[73] Q. Ji et al., Chemical vapour deposition of group-VIB metal dichalcogenide monolayers: engineered substrates from amorphous to single crystalline. Chemical Society Reviews, 44(9) (2015) 2587-2602.
[74] J. C. Shaw et al., Chemical vapor deposition growth of monolayer $MoSe_2$ nanosheets. Nano Research, 7(4) (2014) 511-517.
[75] J. You, , M.D. Hossain, and Z. Luo, Synthesis of 2D transition metal dichalcogenides by chemical vapor deposition with controlled layer number and morphology. Nano Convergence, 5(1) (2018) 1-13.
[76] Y. Peng, , et al., Hydrothermal synthesis and characterization of single-molecular-layer MoS_2 and $MoSe_2$. Chemistry Letters, 30(8) (2001) 772-773.
[77] S. Cao et al., Hydrothermal synthesis of variety low dimensional WS_2 nanostructures. Materials Letters, 129 (2014) 205-208.
[78] O. Rabin et al., An X-ray computed tomography imaging agent based on long-circulating bismuth sulphide nanoparticles. Nature materials,. 5(2) (2006) 118-122.
[79] M.-h. Yao et al., Multifunctional Bi_2S_3/PLGA nanocapsule for combined HIFU/radiation therapy. Biomaterials, 35(28) (2014) 8197-8205.
[80] M. Ma et al., Bi_2S_3-embedded mesoporous silica nanoparticles for efficient drug delivery and interstitial radiotherapy sensitization. Biomaterials,. 37(2015) 447-455.
[81] I. Zafiropoulou et al., In situ deposition and characterization of MoS_2 nanolayers on carbon nanofibers and nanotubes. The Journal of Physical Chemistry C, 117(19) (2013) 10135-10142.
[82] S. Wang, , et al., Biocompatible PEGylated MoS_2 nanosheets: controllable bottom-up synthesis and highly efficient photothermal regression of tumor. Biomaterials, 39(2015) 206-217.
[83] S. Wang et al., A facile one-pot synthesis of a two-dimensional MoS_2/Bi_2S_3 composite theranostic nanosystem for multi-modality tumor imaging and therapy. Advanced materials, 27(17) (2015) 2775-2782.
[84] G. Zhang et al., Shape-dependent defect structures of monolayer MoS_2 crystals grown by chemical vapor deposition. ACS Applied Materials & Interfaces, 9(1) (2017) 763-770.
[85] Y. Zhang et al., Controlled growth of high-quality monolayer WS_2 layers on sapphire and imaging its grain boundary. ACS nano, 7(10) (2013) 8963-8971.
[86] S. Wang et al., Shape evolution of monolayer MoS_2 crystals grown by chemical vapor deposition. Chemistry of Materials, 26(22) (2014) 6371-6379.
[87] A. M.Van Der Zande et al., Grains and grain boundaries in highly crystalline monolayer molybdenum disulphide. Nature materials, 12(6) (2013) 554-561.
[88] A. Govind Rajan et al., Generalized mechanistic model for the chemical vapor deposition of 2D transition metal dichalcogenide monolayers. ACS nano, 10(4) (2016) 4330-4344.
[89] J. Zhang et al., Scalable growth of high-quality polycrystalline MoS2 monolayers on SiO2 with tunable grain sizes. ACS nano, 8(6) (2014) 6024-6030.
[90] Z. Lin et al., Controllable growth of large–size crystalline MoS 2 and resist-free transfer assisted with a Cu thin film. Scientific reports, 5(1) (2015) 1-10.
[91] J. Zhou et al., A library of atomically thin metal chalcogenides. Nature,. 556(7701) (2018) 355-359.
[92] S. Najmaei et al., Vapour phase growth and grain boundary structure of molybdenum disulphide atomic layers. Nature materials, 12(8) (2013) 754-759.
[93] Y. L. Huang et al., Bandgap tunability at single-layer molybdenum disulphide grain boundaries. Nature communications, 6(1) (2015) 1-8.
[94] V. I. Artyukhov et al., Topochemistry of bowtie-and star-shaped metal dichalcogenide nanoisland formation. Nano letters, 16(6) (2016) 3696-3702.
[95] D. Ruzmetov et al., Vertical 2D/3D semiconductor heterostructures based on epitaxial molybdenum disulfide and gallium nitride. Acs Nano, 10(3) (2016) 3580-3588.
[96] L. Chen et al., Step-edge-guided nucleation and growth of aligned WSe_2 on sapphire via a layer-over-layer growth mode. Acs Nano,. 9(8) (2015) 8368-8375.
[97] A. Aljarb et al., Substrate lattice-guided seed formation controls the orientation of 2D transition-metal dichalcogenides. ACS nano, 11(9) (2017) 9215-9222.
[98] Ji, Q., et al., Epitaxial monolayer MoS_2 on mica with novel photoluminescence. Nano letters,. 13(8) (2013) 3870-3877.
[99] Z. Lin et al., Controllable growth of large–size crystalline MoS_2 and resist-free transfer assisted with a Cu thin film. Scientific reports, 5(1) (2015) 1-10.
[100] H. G. Ji et al., Hydrogen-assisted epitaxial growth of monolayer tungsten disulfide and seamless grain stitching. Chemistry of Materials, 30(2) (2018) 403-411.
[101] M. Shanmugam, C.A. Durcan, and B. Yu, Layered semiconductor molybdenum disulfide nanomembrane based Schottky-barrier solar cells. Nanoscale,. 4(23) (2012) 7399-7405.

[102] M. Shanmugam et al., Two-dimensional layered semiconductor/graphene heterostructures for solar photovoltaic applications. Nanoscale,. 6(21) (2014) 12682-12689.
[103] B. Peng, P.K. Ang, and K.P. Loh, Two-dimensional dichalcogenides for light-harvesting applications. Nano Today, 10(2) (2015) 128-137.
[104] A. Pospischil, , M.M. Furchi, and T. Mueller, Solar-energy conversion and light emission in an atomic monolayer p–n diode. Nature nanotechnology, 9(4) (2014) 257-261.
[105] M. M. Furchi et al., Photovoltaic effect in an electrically tunable van der Waals heterojunction. Nano letters, 14(8) (2014) 4785-4791.
[106] O. Lopez-Sanchez et al., Light generation and harvesting in a van der Waals heterostructure. Acs Nano, 8(3) (2014) 3042-3048.
[107] S. W. Tong et al., Graphene intermediate layer in tandem organic photovoltaic cells. Advanced Functional Materials, 21(23) (2011) 4430-4435.
[108] W. Liu et al., PEG-assisted synthesis of homogeneous carbon nanotubes-MoS_2-carbon as a counter electrode for dye-*sensitized solar cells*. Electrochimica Acta, (2014) 119-126.
[109] X. Gu et al., A Solution-processed hole extraction layer made from ultrathin MoS_2 nanosheets for efficient organic solar cells. Advanced Energy Materials, 3(10) (2013) 1262-1268.
[110] S.Q.-u.-A. Naqvi et al. A New WO_3/$FeVO_4$ Nanostructured Heterojunction for Solar-driven Water Oxidation. in IOP Conference Series: Earth and Environmental Science. 2021, IOP Publishing.
[111] C. Lo Vecchio et al., Water Splitting with Enhanced Efficiency Using a Nickel-Based Co-Catalyst at a Cupric Oxide Photocathode. Catalysts, 11(11) (2021) 1363.
[112] M.-Y. Li et al., Epitaxial growth of a monolayer WSe2-MoS2 lateral pn junction with an atomically sharp interface. Science,. 349(6247) (2015) 524-528.
[113] Y. Gong et al., Vertical and in-plane heterostructures from WS2/MoS2 monolayers. Nature materials, 13(12) (2014) 1135-1142.
[114] D. He et al., A van der Waals pn heterojunction with organic/inorganic semiconductors. Appl. Phys. Lett. 107 (2015) 183103.